ChemPhysChem

Research Article
doi.org/10.1002/cphc.202400147

Chemistry Europe
European Chemical Societies Publishing

www.chemphyschem.org

The Effect of Lipopolysaccharides on the Electrostatic Properties of Gram-Negative General Porins from Enterobacteriaceae

Matteo Ceccarelli,*[a] Stefan Milenkovic,[a] and Igor V. Bodrenko[b, c]

We investigated, by using all-atom molecular dynamics simulations, the effect of the outer membrane of Gram-negative bacteria, composed in the outer leaflet by polar/charged lipopolysaccharides (LPS), on the electrostatic properties of general porins from the Enterobacteriaceae family. General porins constitute the main path for the facilitated diffusion of polar antibiotics through the outer membrane. As model system we selected OmpK36 from *Klebsiella pneumoniae*, the ortholog of OmpC from *Escherichia coli*. This species presents high variability of amino acid composition of porins, with the effect to increase its resistance to the penetration of antibiotics. The various properties we analyzed seem to indicate that LPS acts as an independent layer without affecting the internal electrostatic properties of OmpK36. The only apparent effect on the microsecond time scale we sampled is the appearance of calcium ions, when present at moderate concentration in solution, inside the pore. However, we noticed increased fluctuations of the polarization density and only minor changes on its average value.

Introduction

The outer membrane (OM) of Gram-negative bacteria is constituted by two asymmetric layers, the inner leaflet composed by phospholipids and the outer leaflet composed by lipopolysaccharides (LPS) covalently connected to lipids of type A. In addition to the hydrophobicity character of these layers, the additional LPS confers an increased thickness to the membrane, constituting, as a whole, a real physical barrier for fast direct diffusion of any molecule, hydrophilic or hydrophobic.[1]

The permeability of the outer membrane is thus specifically controlled by the expression of various porins, with different composition and numbers,[2] representing a facilitated path for diffusing molecules through the outer membrane.[3] In particular, in the Enterobacteriaceae family the presence of trimeric general porins, such as OmpF and OmpC from *Escherichia coli*, provides a not specific path for polar molecules to enter the cell.[4] It was demonstrated that these porins constitute an effective path for polar anti-infectives to reach internal targets: beta lactams, fluoroquinolones, small aminoglycosides as well inhibitors.[5–8] Reconstituted experiments in black lipid membranes (BLM) demonstrated that polar antibiotics, under an effective gradient concentration, can diffuse through porins with flux in the range from 1 to 1000 molecules per seconds.[9–11] These results were complemented by all-atom molecular dynamics simulations that proposed a molecular mechanism and confirmed the effectiveness of general porins to help the diffusion of polar anti-infectives.[12–14] However, both methods have made use of symmetric bilayers composed of various phospholipids. Simulations with complete LPS are challenging for several reasons. The LPS architecture, its thickness, chemical composition, and density depends on species and inside a single species on strains.[15] The presence of divalent cations is another concern for its difficulty to describe them with empirical potentials.[16] Additionally, the large number of atoms is another limiting factor for the long simulations required to achieve an equilibrated complex membrane protein-LPS.[17]

The initial attempt to explicitly model LPS allowed simulations of systems composed of a few units for less than 10 ns.[18,19] Only recently have they become affordable and able to provide microsecond trajectories within a reasonable timeframe.[20,21] At the same time, recent electrophysiology experiments using LPS have revealed some differences compared to data acquired with symmetric bilayers.[22] Thus, many aspects and mechanisms proposed in the past for small-molecule diffusion need to be reviewed through the use of all-atom molecular dynamics simulations.

We focused our attention to bacteria from the Enterobacteriaceae family, expressing two trimeric general porins. These porins share two structural features: [23] (i) an hourglass shape, due to the internal folding of the long loop L3 that

[a] M. Ceccarelli, S. Milenkovic
Department of Physics, University of Cagliari, Cittadella Universitaria, 09042 Monserrato (IT)
E-mail: matteo.ceccarelli@dsf.unica.it

[b] I. V. Bodrenko
Istituto Nanoscienze, CNR, piazza San Silvestro 12 56127, Pisa, Italy

[c] I. V. Bodrenko
Lab NEST, Scuola Normale Superiore, piazza San Silvestro 12 56127, Pisa, Italy

Supporting information for this article is available on the WWW under https://doi.org/10.1002/cphc.202400147

creates the so-called constriction region; (ii) the separation of charges at the constriction region, with basic amino acids on one side facing the acidic amino acids of the loop L3. The latter feature creates an electric field, as postulated many years ago.[24,25] Because these porins are classified as water-filled channels, the presence of water inside the monomers permitted us to develop a new method for quantify the macroscopic internal electric field, using water molecules as a probe.[26] We quantified the presence of a strong macroscopic transversal electric field, around 30 mV/Å, and we demonstrated it is able to influence the diffusion of dipolar antibiotics.[27,28] The LPS layer has a high negative charge and divalent counterions (magnesium and calcium) are present to neutralize it. As shown in the past, the presence of divalent cations can change the selectivity of the pore and thus interfere with the diffusion of ions and antibiotics.[29–32] The lack of good parameters for describing divalent cations did not permit to have high accuracy and thus predictivity power with molecular simulations. Here we employed the recent multi-site model of calcium designed to reproduce binding energies with proteins and residence time of water molecules.[33–35]

Our aim is to show at which extent the presence of a charged layer as LPS and divalent cations can affect the electric field inside porins, and thus the diffusion of antibiotics. As porin model we considered the OmpC ortholog from *Klebsiella pneumoniae*, OmpK36. This species attracted many interests in the last years since it is capable to resist to the antibiotics by modifying its permeability acting directly on porins, either varying their expression or through amino acids substitutions/insertions.[36–39]

Methods

We prepared the model systems starting from the high-resolution structure obtained by X-ray diffraction, PDBID 6RD3, at 1.98 Å.[40] By employing the CHARMM-GUI web tool,[41–43] we embedded the trimer in the asymmetric bilayer (150×150 Å), with calcium ions to neutralize LPS molecules and solvated with water at 0.15 M KCl. For the protein, membrane, ions and LPS we used the charmm36 m force field, and TIP3P[44] for water. For calcium we used the recent 7-site model able to better reproduce the interactions with proteins and water.[33,34] We protonated one residue behind the loop L3, as proposed in the past[45] and as suggested by the software Propka (Asp-297). *Inner leaflet:* we followed the suggestion of the Ref.[46] (*http://www.ks.uiuc.edu/Training/Tutorials/)*, adding PVCL2, PMPE, PMPG, PVPE, and PVPG with ratio (2:8:1:8:2). *Outer leaflet:* we prepared LPS from the E.coli,[47] Type1 lipid A, R1 core, 3 O-units (O1), with no chemical modification. We also prepared LPS from K.pneumoniae,[48] A core, 3 O-units (O1-1), also in this case with no chemical modifications. In both cases, LPS covers homogeneously the surface. See Figure S1 for more information on the two LPS systems.

All systems were equilibrated initially by the CHARMM-GUI tool,[41–43] then we followed the protocol proposed using the simulations reported in Table 1, before the production runs.

The final equilibrated systems have approx. 457000 and 370000 atoms, respectively for *E.coli* (EC) and *K.pneumoniae* (KP) LPS systems. All simulations were performed with the CPU/GPU 2022 version of the Gromacs package.[49–52] A time step of 2 fs was employed with LJ cutoff at 12 Å and PME for treating long range electrostatic interactions. Because of the long relaxation required for such complex system,[53,54] we used the last 500 ns for data analysis.

We compared the KP and EC systems with the model embedding OmpK36 in a POPC symmetric bilayer.[23] We used the same force field parameters and followed the same protocol. The final system has approx. 118000 atoms (0.15 M KCl) in a box of 10.8×10.8×9.7 nm^3. See Figure 1 for a comparison of the three model systems.

Table 1. Runs performed for equilibration and production for all simulated models (BB = backbone; SC = side chains).

Length	Constraints BB/SC/LIPIDS	Temperature	Algorithm	Pressure	Algorithm
EQUILIBRATION					
5000 steps	4000/2000/1000	Minimization			
125 ps	4000/2000/1000	300 K	Berendsen	NVT	NA
125 ps	2000/1000/400	300 K	Berendsen	NVT	NA
125 ps	1000/500/400	300 K	Berendsen	Semiisotropic	Berendsen
500 ps	500/200/200	300 K	Berendsen	Semiisotropic	Berendsen
500 ps	200/50/40	300 K	Berendsen	Semiisotropic	Berendsen
500 ps	50/0/0	300 K	Berendsen	Semiisotropic	Berendsen
30 ns	NO	300 K	V-rescale	Semiisotropic	Parrinello-Rahman
PRODUCTION					
500 ns	NO	300 K	V-rescale	Semiisotropic	Parrinello-Rahman
500 ns	NO	300 K	V-rescale	Semiisotropic	Parrinello-Rahman

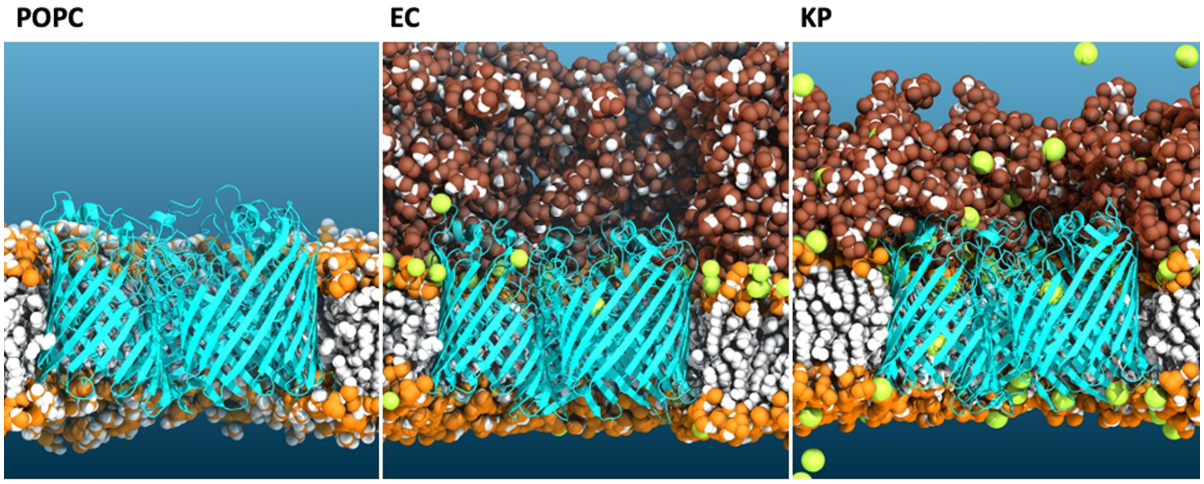

Figure 1. Side view of the three model systems of the trimeric OmpK36 embedded in membrane of different complexity. From left to right: inside a symmetric POPC bilayer; inside the LPS from E. coli; inside the LPS from K pneumoniae. The yellow spheres represent the calcium ions added to neutralize LPS molecules. Snapshots are taken from the end of the respective molecular dynamics production trajectories.

Results

The facilitated transport of molecules through pores is determined by diffusion upon a gradient concentration.[55,56] One of the questions raised when investigating the antibiotics diffusion through bacterial porins was the possible obstruction represented by the movement of the flexible long sugar chains above the porin's mouth,[20] see Figure 1. The models prepared in a symmetric bilayer to mimic electrophysiology experiments with BLM cannot catch it.[23,28]

The external radius of the trimer is approximately 35 Å and the internal radius 25 Å, due to the internal folding of the loop L3. In order to evaluate the presence of LPS above the porin's mouth, we considered cylinders with radii from 10 to 35 Å and width 1.0 Å, centered on the trimer (check Figure S2 for dimensions of the trimer and water cylinders). By calculating the number of water molecules in such cylinders, as function of the position Z, we can evaluate at which extent the LPS obstruct the region above the trimer ($30\ \text{Å} < Z < 60/80\ \text{Å}$) looking at the difference with the number of water molecules in the bulk region. As we can see from Figure 2, the LPS starts constricting slightly the mouth region with a radius of 25 Å, and more pronounced at higher radii, especially for system EC with respect to KP. In particular, the EC model system shows a constant obstruction along Z in the core region for radii larger than 25 Å, and then a funnel-like obstruction for the O-antigen region. The opposite we have for KP, with a funnel-like obstruction for the core region, and not any obstruction for the short O-antigen region.

Another aspect one could not consider when modelling the trimer in the symmetric bilayer was the effect of the many additional negative charges the LPS brings. Each lipid A has two phosphate (−4e) and the long sugar chains can have additional negative charges (carboxilic groups) and sometimes positive charges (amine groups). These charges are neutralized by dications (Mg^{2+} and Ca^{2+}) that act as glue for stabilizing chains.[57] It is well known that chelators of dications provoke a damage to the outer membrane, making it more permeable.[1,57] For system EC we added 3 calcium ions per lipid A to neutralize the −6e charge of each chain. On the other hand, the structure of LPS from K.pneumoniae, the KP model, has −9e charge per chain, requiring a higher number of calcium ions for neutralization, 5 per chain. In addition, we added KCl at concentration of 0.15 M. We calculated the density of ions in two regions: (i) above/below and inside the trimer region, within a cylinder of radius 25 Å centered on the trimer; (ii) outside the trimer region in the region limited by two radii, $40\ \text{Å} < R < 70\ \text{Å}$, above/below and at the LPS region.

Ions Density

The calcium density was calculated only for the two LPS model systems since calcium was not added to the bilayer (POPC) system, see Figure 3. The number of calcium ions is much larger in the KP than the EC model system. Thus, in the former, we observe calcium ions also in the bulk, whereas they are almost absent in the EC model. Similarly, only the KP system displays calcium ions along the entire length of the trimer, whereas in the EC system calcium ions are observed only in the central region of the protein, $Z = 5$ Å.

If we look at densities outside the trimer (right in Figure 3), the calcium ions occupy the region above the lipid A (centered at $Z = 12$ Å from the center of the trimer), where phosphate groups are localized in the LPS, and with a lower peak at the membrane surface of the inner leaflet (centered $Z = -25$ Å), because of the negative charge of some phospholipid headgroups. The calcium density for model KP shows an additional peak around $29\ \text{Å} < Z < 33\ \text{Å}$, due to the structural difference of the two sugar chains and localization of charged groups, see Figure S1.

The density of potassium/chloride along Z, ρ_Z, was transformed into a free energy difference with respect to the bulk density using the formula:

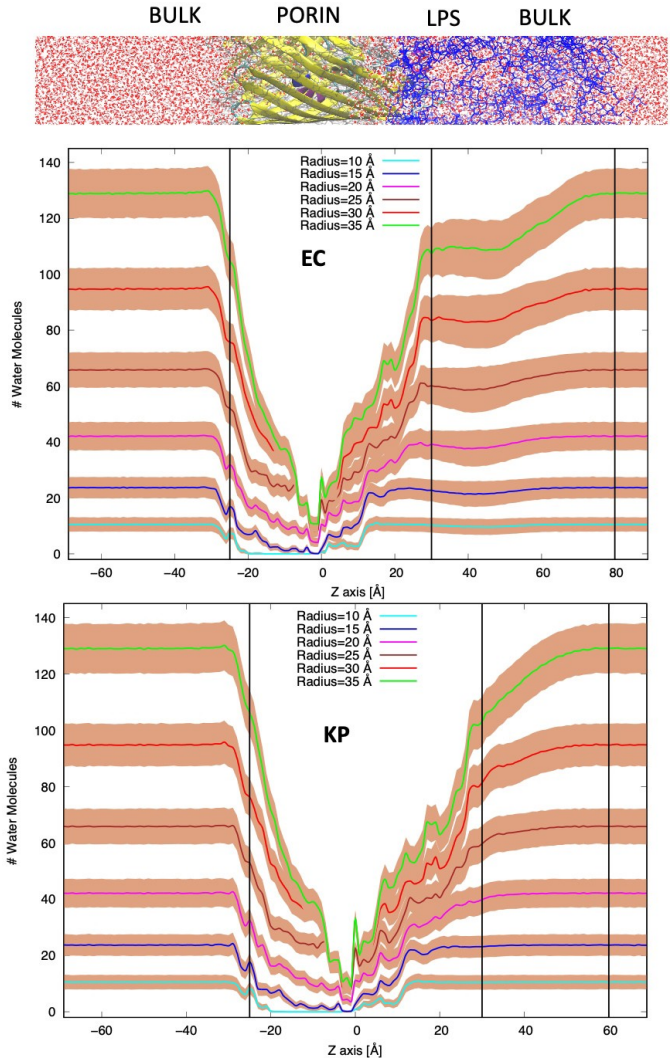

Figure 2. Number of average water molecules calculated inside cylinders of increased radius all centered on the trimer and moving along the Z axis ($\triangle Z = 1$ Å). The shaded regions represent the variance. The black vertical lines divide the region along Z, as reported on top: from left the bulk water (red and white), the porin (yellow), the LPS (blue) and again the bulk water.

$$\Delta G(Z) = -k_B T \, ln\left(\frac{\rho_Z}{\rho_{bulk}}\right) \quad (1)$$

and reported in Figure S4/S5 with data from the POPC model system too. When focusing on the two LPS model systems, both ion species show a positive free energy difference, indicating that they do not enter either the trimer or the LPS, apart the single binding site for potassium, at the constriction region of the trimer in the EC model system. It is noteworthy that the free energy difference is higher for chloride than for potassium. The repulsion for chloride can be explained by the prevalence of negative charges in both the trimer and LPS. Additionally, potassium compete with calcium ions to occupy the trimer. Consequently, the free energy for potassium is higher in the KP model than in the EC model because the former contains more calcium ions inside the porin. To confirm the correctness of this analysis we can compare the two systems with the POPC system, without calcium. POPC free energy differences of both chloride and potassium are more similar to EC, and for the latter we have the same binding site for potassium at $Z = -2$ Å.

Internal Electric Field

In order to evaluate the macroscopic internal electric field, we employed as probe the polarization density of water molecules inside a sphere of radius 5 Å. We identified and moved the probe along Z in each of the three monomers, from -25 Å $< Z < 30$ Å, and outside this range centered on the center of mass of the trimer. The calculated polarization density of the probe is reported in Figure 4, as the average of the three monomers of each model system.

The comparison with the POPC system and the two models with LPS shows that there is no a large effect of LPS on the average polarization density inside the monomers. If we look at the transversal component, the highest peak is located exactly at the constriction region, the center region of the pore, and a less prominent peak is visible on the extracellular side just next to the constriction region, that we termed the preorientation region.[23,27] The shades regions of the three curves indicate the maximum-minimum difference of polarization density in the three monomers. We can see how the model KP has the highest variation in the three monomers, and the POPC model shows slightly large value at the two peak regions. The transversal polarization density above the mouth's trimer (dotted line), the water region surrounded by LPS, is zero, as expected by considering its symmetry.

The longitudinal component of the polarization density inside the three monomers is much smaller than the transversal component, in agreement with previous calculations on other porins of the same family.[23,26] Interestingly, outside the trimer we see a non-vanishing component at around $Z = -25$ Å and $Z = 20$ Å, corresponding to the two regions where the three monomers are in contact. The opposite directions of the polarization density mean an electric field pushing from both sides a positively charged probe inside the pore, whose total charge is negative. Also, the longitudinal component is zero in the LPS-surrounded region ($Z > 30$ Å). The only noticeable fact is the lack of polarization density for KP above the trimer at $Z = 20$ Å. This region shows a density of calcium ions higher for KP than for EC (Figure 3), thus able to neutralize the effect of the negative charge of the pore.

Structural Flexibility

We evaluated the structural flexibility of the porin by calculating the root mean square fluctuations of all residues in the three model systems, highlighting the loops of the extracellular mouth, see Figure 5, more interesting for potential interactions with molecules arriving from the extracellular side. Some marked differences are visible for the L3 and L4 loops. In the

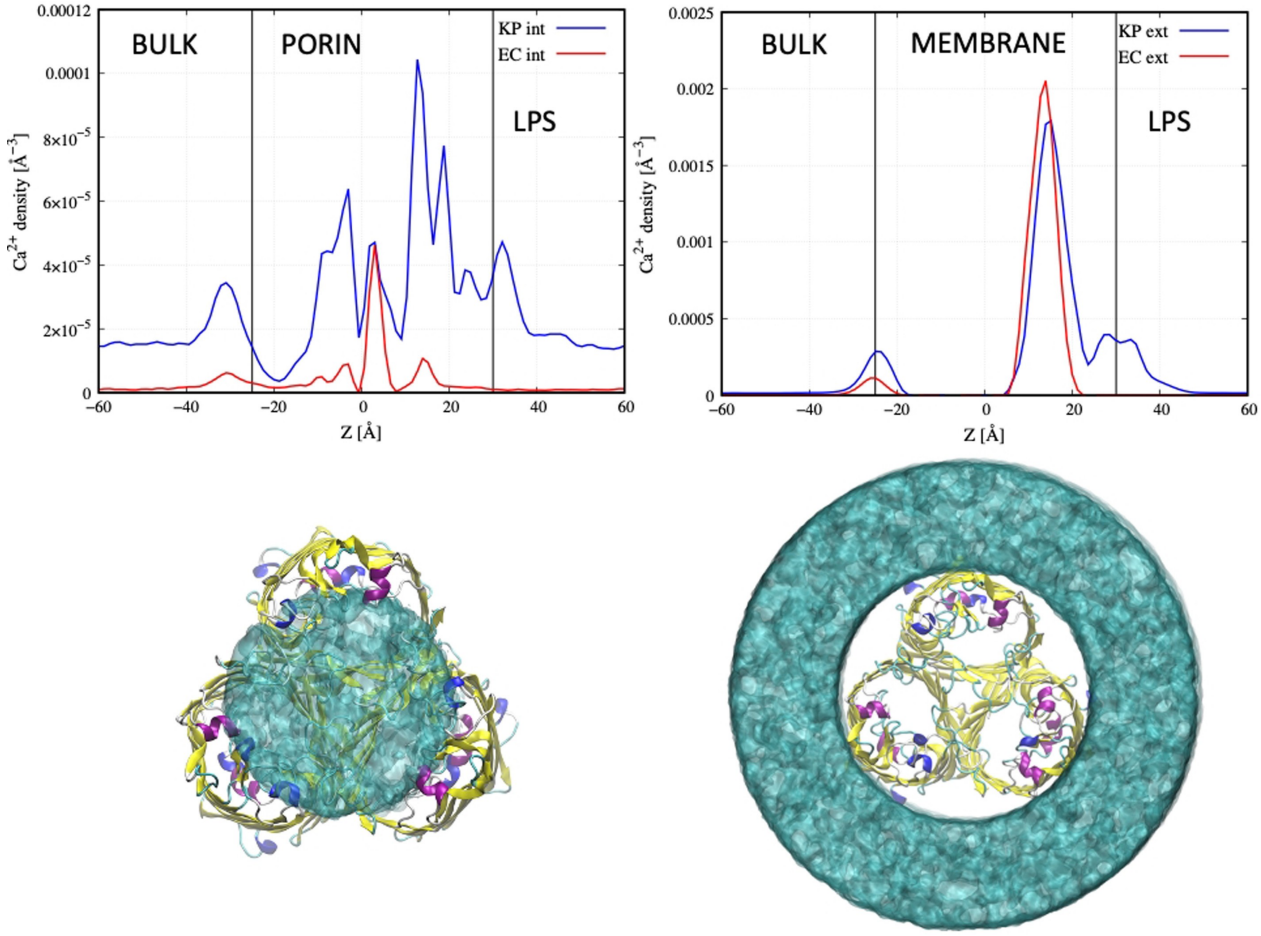

Figure 3. Density of calcium ions versus position along the axis Z respectively inside the trimer (left, cylinder of R = 25 Å represented below) and outside the trimer (right, region 40 Å < R < 70 Å, represented below). The black lines indicate approximately the three regions of interest, respectively the bulk, the porin/membrane, and the LPS region.

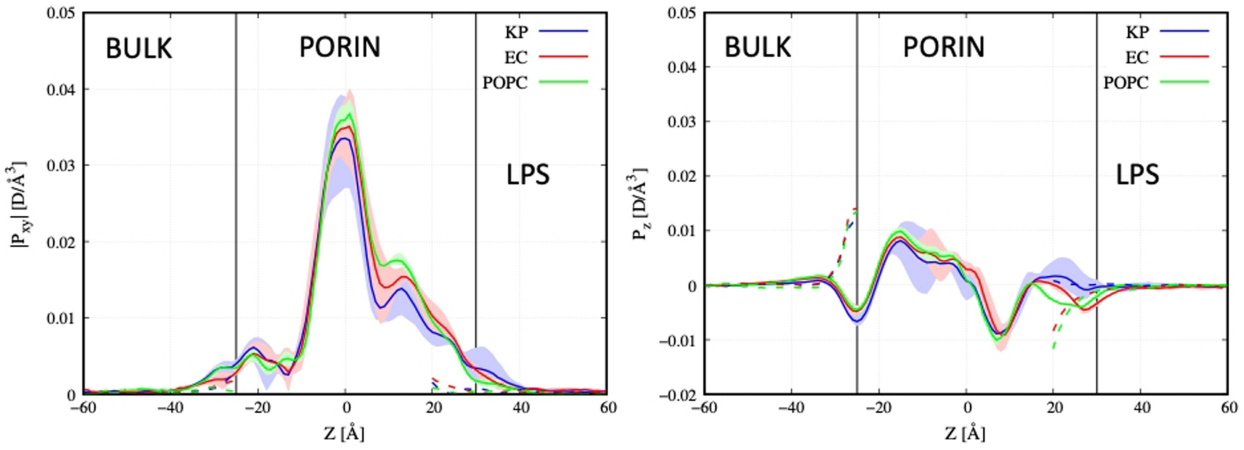

Figure 4. Transversal (left) and longitudinal (right) polarization density inside the three monomers (straight lines) and outside the trimer (dotted lines) for the three model systems. The black lines indicate approximately the three regions of interest, respectively the bulk, the porin, and the LPS region.

model system KP the L3 has large fluctuations compared to the other two model systems. However, the highest fluctuations are in L4, more for EC than KP and POPC. Interestingly, from Figure 5-B we see that this loop is at the invagination of two monomers.

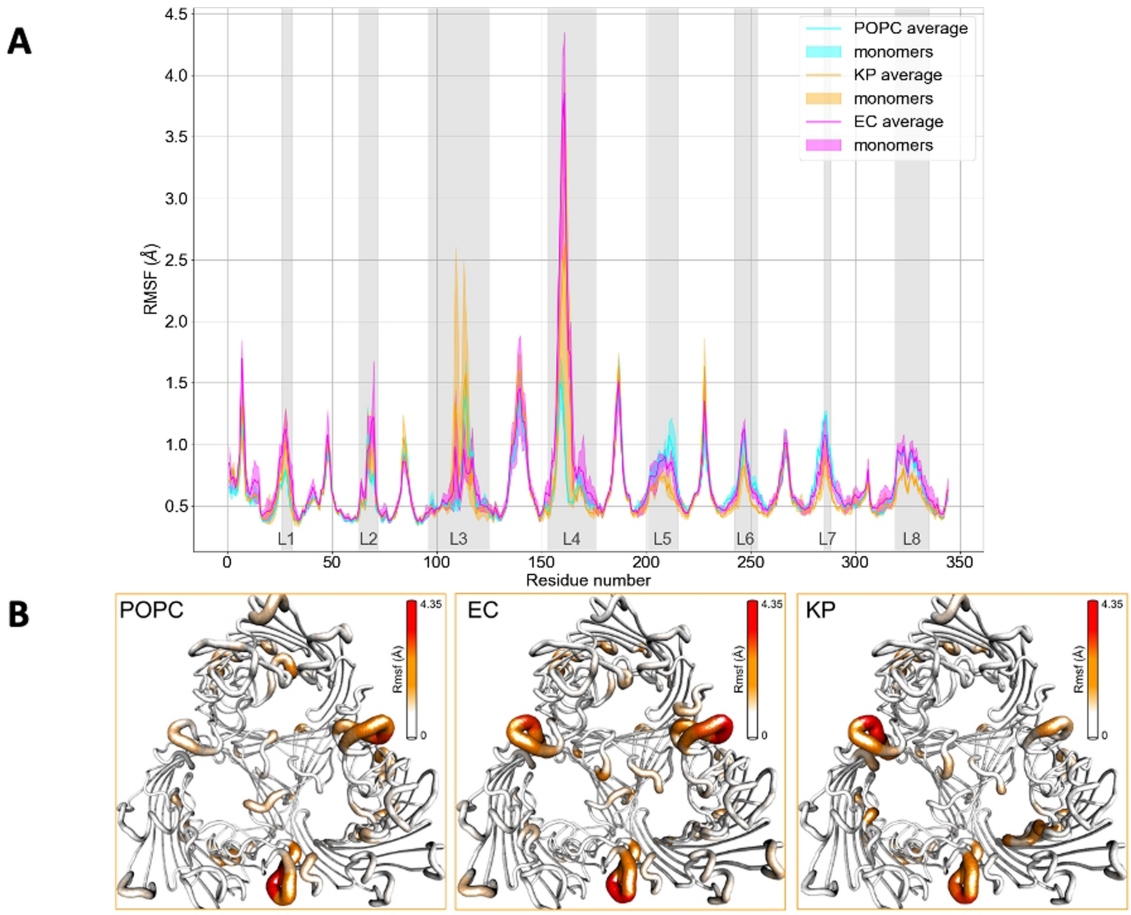

Figure 5. (A) RMSF per residue of each monomer and for the three systems. In gray the loops facing the extracellular mouth. The straight lines represent the average of the three monomers, the shaded regions indicate the maximum-minimum RMSF of the three monomers (B) Top view of the trimer in the three model systems represented as tube. The color and size of tubes are proportional to the RMSF.

Discussion

We analyzed two homogeneous LPS structures with different complexity, the EC model with few charges in the core region and a long O-antigen region, and the KP model with more charges in the core region and a short O-antigen region (see Figure S2). The KP system, having more charges, has also a high number of neutralizing calcium ions. In addition, because of the procedure used by CHARMM-gui for neutralizing the LPS chains, we have more calcium in KP system than the necessary ions to neutralize the charge of the entire LPSs. Thus, this system is functional to evaluate the effects of calcium excess in solution.

We analyzed the obstruction of the region above the extracellular mouth of the channel by calculating the average number of water molecules in increasing-size cylinders placed parallel to the Z axis. Our results indicate that only for radii larger than 25 Å we start to see obstruction, and at different extent for the EC and KP model systems (Figure 2). In the former the obstruction is constant in the core region and decreases at the level of the O-antigen in a funnel-like manner. In the latter, we have instead a funnel-like obstruction for the core region at varying Z and no obstruction for the short O-antigen region. We can ascribe this to the different structures of the two LPS chains. The charged groups all along the entire core region in KP (Figure S2) attract calcium ions, as visible from the second peak of the density at around Z = 30 Å (Figure 3). It is well known from previous investigations that calcium works as glue for LPS,[57] and from our analysis we can add that it avoids the collapse of LPS chains over the external loops of the pore. However, we think that small molecules like polar antibiotics that use porins to cross the OM can diffuse almost freely in a cylinder of radius 25 Å, being the constriction region of the pore much more important for modulating the rate of transport.[58] This value is key because it represents exactly the radius for accessing the three monomers, as shown in Figure S2. This result seems partially in contrast with a previous investigation that used shorter simulations and slightly different construct for the LPS.[20] Inhomogeneity of LPS density on the flexibility and thus its effect on pore occlusion should be tested more systematically in future. We can conclude that more charged groups in LPS favor proper LPS-LPS interactions avoiding the collapse toward the trimer, that would inhibit important functional interaction of loops with molecules from the extracellular side.[59,60]

The comparison of the polarization density of our water probe for the three systems showed that the presence of LPS

and calcium ions has only minor effects on both the transversal and longitudinal components inside the monomers, Figure 4. Moreover, the polarization density above the extracellular mouth, that region surrounded by LPS chains and calcium ions, is zero, as expected also by symmetry. We noticed instead some differences in the polarization density inside each monomer, especially for KP system. As we said this model system is the one with an excess of calcium. Looking at the density of ions (Figure 3), we saw that more calcium is present inside the negatively charged trimer, above and below the central constriction region. This excess of calcium has two effects: (i) on one side it alters the polarization density and thus the electric field; its effect is not so strong to change the average, rather it creates larger variations between the minimum and maximum values calculated for the three monomers (shaded area in Figure 4). Interestingly, an increase of fluctuations was observed experimentally measuring ionic current through OmpF in presence of LPS.[22] (ii) On the other, it repels potassium ions from inside the trimer. The free energy difference of potassium with respect to the bulk (Figure S4) is similar for POPC and EC models, and different for KP. Further, the chloride free energy difference is less positive for KP versus EC and POPC, probably due to less repulsion of chloride by calcium ions present inside the trimer. Future simulations with an external electric field might verify if the excess calcium is enough to give a change in selectivity, as shown in electrophysiology using a symmetric bilayer.[29,30,61] We know that an external electric field can induce pore gating, as observed experimentally at voltages as low as 200 mV.[62] In simulations, however, we can reach up to 1 V, resulting in few observable gating events on the microsecond timescale, particularly with mutants.[63] Ultimately, only simulations employing an external electric field combined with enhanced sampling techniques may elucidate the gating mechanism at low voltages and determine whether it is influenced by the presence of divalent cations.

The more flexible elements, the loops, were analyzed by calculating the root mean square fluctuations. We noticed that the external loop with the highest flexibility is the L4, located at the invagination of two monomers. Interestingly, in this region was found one of the two binding sites for LPS in the crystal structure of OmpE36,[17,64] the ortholog of our pore in *Enterobacter aerogenes*. In light of what we found we can speculate that the large flexibility of this region might help LPS to find an optimal binding with the pore. Moreover, the invagination is also by construction a region offering a larger surface for interactions with a molecule, thus this result is not surprising us.

To summarize, the picture that emerges is that the strength of obstruction by LPS depends on the structure of LPS chains and its charged groups, but it should not be able to have a direct effect on the diffusion of small polar antibiotics, perhaps for the interaction with larger macromolecules. The LPS itself does not interfere with the electrostatic properties of the trimer, that maintains its features, as shown in the past key for transport of small molecules. The most important fact is the effect due to the attraction of calcium ions, when present at moderate concentration in solution, though the presence of calcium ions is able to increase only the fluctuations of the polarization density inside, without affecting the average values. Thus, the LPS seems to act as an independent layer with its own properties to filter/decrease the direct diffusion of molecules toward the periplasm, without interference with the electrostatic properties of the embedded porins.

Acknowledgements

We acknowledge the CINECA award under the ISCRA initiative, for the availability of high-performance computing resources and support through the project "Strict" run on the Leonardo supercomputer. This research was partially supported by EU funding within the NextGeneration EU-MUR PNRR Extended Partnership initiative on Emerging Infectious Diseases (Project no. PE00000007, INF-ACT) Open Access publishing facilitated by Università degli Studi di Cagliari, as part of the Wiley - CRUI-CARE agreement.

Conflict of Interests

The authors declare no conflict of interest.

Data Availability Statement

The data that support the findings of this study are available from the corresponding author upon reasonable request.

Keywords: Bacterial porins · LPS · Klebsiella Pneumoniae · Molecular Dynamics Simulations · Electric Field

[1] H. Nikaido, *Microbiol. Mol. Biol. Rev.* **2003**, *67*, 593–656.
[2] H. Nikaido, *J. Bacteriol.* **1983**, *153*, 241–252.
[3] A. H. Delcour, *Front. Biosci.* **2003**, *8*, d1055–71.
[4] S. Kojima, H. Nikaido, *Proc. Natl. Acad. Sci. USA* **2013**, *110*, E2629–34.
[5] F. Yoshimura, H. Nikaido, *Antimicrob. Agents Chemother.* **1985**, *27*, 84–92.
[6] T. Mach, P. Neves, E. Spiga, H. Weingart, M. Winterhalter, P. Ruggerone, et al., *J. Am. Chem. Soc.* **2008**, *130*, 13301–13309.
[7] J. Vergalli, I. V. Bodrenko, M. Masi, L. Moynié, S. Acosta-Gutierrez, J. H. Naismith, et al., *Nat. Rev. Microbiol.* **2020**, *18*, 164–176.
[8] J. A. Bafna, E. Sans-Serramitjana, S. Acosta-Gutierrez, I. V. Bodrenko, D. Hörömpöli, A. Berscheid, et al., *ACS Infect. Dis.* **2020**, *6*, 1855–1865.
[9] M. Masi, J. Vergalli, I. Ghai, A. Barba-Bon, T. Schembri, W. M. Nau, et al., *Commun. Biol.* **2022**, *5*, 1059.
[10] I. Ghai, A. Pira, M. A. Scorciapino, I. Bodrenko, L. Benier, M. Ceccarelli, F. Omp, *J. Phys. Chem. Lett.* **2017**, *8*, 1295–1301.
[11] I. Bodrenko, H. Bajaj, P. Ruggerone, M. Winterhalter, M. Ceccarelli, *Analyst* **2015**, *140*, 4820–4827.
[12] J. D. Prajapati, C. J. F. Solano, M. Winterhalter, U. Kleinekathöfer, *J. Phys. Chem. B* **2018**, *122*, 1417–1426.
[13] A. Pira, M. A. Scorciapino, I. V. Bodrenko, A. Bosin, S. Acosta-Gutierrez, M. Ceccarelli, *Molecules* **2020**, *25*, 5747.
[14] G. M. Tuveri, M. Ceccarelli, A. Pira, I. V. Bodrenko, *Antibiotics* **2022**, *11*, 840.
[15] C. Whitfield, N. Kaniuk, E. Frirdich, *J. Endotoxin Res.* **2003**, *9*, 244–249.
[16] T. Martinek, E. Duboué-Dijon, Š. Timr, P. E. Mason, K. Baxová, H. E. Fischer, et al., *J. Chem. Phys.* **2018**, *148*, 222813–10.
[17] A. Kesireddy, K. R. Pothula, J. Lee, D. S. Patel, M. Pathania, B. van den Berg, et al., *J. Phys. Chem. B* **2019**, *123*, 5700–5708.

[18] R. D. Lins, *Biophys. J.* **2001**, *81*, 1037–1046.
[19] T. P. Straatsma, T. A. Soares, *Proteins* **2009**, *74*, 475–488.
[20] D. S. Patel, S. Re, E. L. Wu, Y. Qi, P. E. Klebba, G. Widmalm, et al., *Biophys. J.* **2016**, *110*, 930–938.
[21] J. Lee, K. R. Pothula, U. Kleinekathöfer, W. Im, *J. Phys. Chem. B* **2018**, *122*, 8185–8192.
[22] J. Wang, R. Terrasse, J. A. Bafna, L. Benier, M. Winterhalter, *Angew. Chem. Int. Ed. Engl.* **2020**, *59*, 8517–8521.
[23] S. Acosta-Gutierrez, L. Ferrara, M. Pathania, M. Masi, J. Wang, I. Bodrenko, et al., *ACS Infect. Dis.* **2018**, *4*, 1487–1498.
[24] A. Karshikoff, V. Spassov, S. W. Cowan, R. Ladenstein, T. Schirmer, *J. Mol. Biol.* **1994**, *240*, 372–384.
[25] K. M. Robertson, D. P. Tieleman, *FEBS Lett.* **2002**, *528*, 53–57.
[26] S. Acosta-Gutierrez, I. Bodrenko, M. A. Scorciapino, M. Ceccarelli, *Phys. Chem. Chem. Phys.* **2016**, *18*, 8855–8864.
[27] S. Acosta-Gutierrez, M. A. Scorciapino, I. Bodrenko, M. Ceccarelli, *J. Phys. Chem. Lett.* **2015**, *6*, 1807–1812.
[28] H. Bajaj, S. Acosta-Gutierrez, I. Bodrenko, G. Malloci, M. A. Scorciapino, M. Winterhalter, et al., *ACS Nano* **2017**, *11*, 5465–5473.
[29] A. Alcaraz, E. M. Nestorovich, M. L. López, E. García-Giménez, S. M. Bezrukov, V. M. Aguilella, *Biophys. J.* **2009**, *96*, 56–66.
[30] P. R. Singh, M. Ceccarelli, M. Lovelle, M. Winterhalter, *J. Phys. Chem. B* **2012**, *116*, 4433–4438.
[31] B. Dhakshnamoorthy, B. K. Ziervogel, L. Blachowicz, B. Roux, *J. Am. Chem. Soc.* **2013**, *135*, 16561–16568.
[32] L. G. M. Ferrara, G. D. Wallat, L. Moynié, N. N. Dhanasekar, S. Aliouane, S. Acosta-Gutierrez, et al., *J. Mol. Biol.* **2016**, *428*, 4528–4543.
[33] A. Zhang, H. Yu, C. Liu, C. Song, *Nat. Commun.* **2020**, *11*, 922.
[34] C. Liu, A. Zhang, N. Yan, C. Song, *J. Phys. Chem. Lett.* **2021**, *12*, 4286–4291.
[35] C. M. Ives, N. J. Thomson, U. Zachariae, *J. Gen. Physiol.* **2023**, *155*, e202213226.
[36] J. L. C. Wong, S. David, J. Sanchez-Garrido, J. Z. Woo, W. W. Low, F. Morecchiato, et al., *Proc. Nat. Acad. Sci.* **2022**, *119*, e2203593119.
[37] S. David, J. L. C. Wong, J. Sanchez-Garrido, H.-S. Kwong, W. W. Low, F. Morecchiato, et al., *PLoS Pathog.* **2022**, *18*, e1010334.
[38] N. C. Rosas, J. Wilksch, J. Barber, J. Li, Y. Wang, Z. Sun, et al., *eLife* **2023**, *12*, e83107.
[39] M. Wang, Y. Tian, L. Xu, F. Zhang, H. Lu, M. Li, et al., *Microbiol Spectr* **2022**, 10, e00507–22.
[40] J. L. C. Wong, M. Romano, L. E. Kerry, H.-S. Kwong, W. W. Low, S. J. Brett, et al., *Nat. Commun.* **2019**, *10*, 3957–10.
[41] S. Jo, T. Kim, V. G. Iyer, W. Im, *J. Comput. Chem.* **2008**, *29*, 1859–1865.
[42] S. Jo, J. B. Lim, J. B. Klauda, W. Im, *Biophys. J.* **2009**, *97*, 50–58.
[43] J. Lee, X. Cheng, J. M. Swails, M. S. Yeom, P. K. Eastman, J. A. Lemkul, et al., *J. Chem. Theory Comput.* **2016**, *12*, 405–413.
[44] W. L. Jorgensen, J. Chandrasekhar, J. D. Madura, R. W. Impey, *J. Chem. Phys.* **1983**, *79*, 926.
[45] S. Varma, S.-W. Chiu, E. Jakobsson, *Biophys. J.* **2006**, *90*, 112–123.
[46] Y. Li, J. Liu, J. C. Gumbart, *Methods Mol. Biol.* **2021**, *2302*, 237–251.
[47] Y. Liu, G. B. Koudelka, *Microbiol Spectr* **2023**, *11*, e02930–22.
[48] E. Vinogradov, E. Frirdich, L. L. MacLean, M. B. Perry, B. O. Petersen, J. Ø. Duus, et al., *J. Biol. Chem.* **2002**, *277*, 25070–25081.
[49] E. Lindahl, B. Hess, *J. Mol. Model.* **2001**, *7*, 306–317.
[50] D. V. D. Spoel, E. Lindahl, B. Hess, G. Groenhof, A. E. Mark, H. J. C. Berendsen, *J. Comput. Chem.* **2005**, *26*, 1701–1718.
[51] M. J. Abraham, T. Murtola, R. Schulz, S. Páll, J. C. Smith, B. Hess, et al., *SoftwareX* **2015**, *1–2*, 19–25.
[52] J. Lee, X. Cheng, J. M. Swails, M. S. Yeom, P. K. Eastman, J. A. Lemkul, et al., *J. Chem. Theory Comput.* **2016**, *12*, 405–413.
[53] K. N. Kirschner, R. D. Lins, A. Maass, *J. Chem. Theory Comput.* **2012**, *8*, 4719–4731.
[54] J. Shearer, D. Jefferies, S. Khalid, *J. Chem. Theory Comput.* **2019**, *15*, 2608–2619.
[55] M. A. Scorciapino, S. Acosta-Gutierrez, D. Benkerrou, T. D'Agostino, G. Malloci, S. Samanta, et al., *J. Phys. Condens. Matter* **2017**, *29*, 113001.
[56] A. M. Berezhkovskii, M. A. Pustovoit, *J. Chem. Phys.* **2002**, *116*, 9952–9956.
[57] L. A. Clifton, M. W. A. Skoda, A. P. L. Brun, F. Ciesielski, I. Kuzmenko, S. A. Holt, et al., *Langmuir* **2015**, *31*, 404–412.
[58] S. Milenkovic, J. Wang, S. Acosta-Gutierrez, M. Winterhalter, M. Ceccarelli, *Phys. Chem. Chem. Phys.* **2023**, *25*, 12712–12722.
[59] Q.-T. Tran, L. Maigre, T. D'Agostino, M. Ceccarelli, M. Winterhalter, J.-M. Pagès, et al., *Res. Microbiol.* **2017**, *168*, 685–699.
[60] R. A. Dunstan, R. S. Bamert, K. S. Tan, U. Imbulgoda, C. K. Barlow, G. Taiaroa, et al., *Cell Rep.* **2023**, *42*, 112551.
[61] M. L. López, E. García-Giménez, V. M. Aguilella, A. Alcaraz, *J. Phys. Condens. Matter* **2010**, *22*, 454106.
[62] E. M. Nestorovich, *Int. J. Mol. Sci.* **2023**, *24*, 16655.
[63] A. Acharya, I. Ghai, C. Piselli, J. D. Prajapati, R. Benz, M. Winterhalter, et al., *J Chem Inf Model* **2022**, *63*, 910–927.
[64] W. Arunmanee, M. Pathania, A. S. Solovyova, A. P. L. Brun, H. Ridley, A. Baslé, et al., *Proc. Nat. Acad. Sci.* **2016**, *113*, E5034–E5043.

Manuscript received: February 8, 2024
Revised manuscript received: April 15, 2024
Accepted manuscript online: April 16, 2024
Version of record online: May 27, 2024